Journal of Tissues and Materials

Characterization of the Precipitated Dicalcium Phosphate Dehydrate on the Graphene Oxide Surface as a Bone Cement Reinforcement

Hassan Nosrati[1], **Dang Quang Svend Le**[2], **Reza Zolfaghari Emameh**[3], **Cody Eric Bunger**[2]

[1]Department of Materials Engineering, Tarbiat Modares University, Tehran, Iran
[2]Department of Clinical Medicine, Aarhus University, Denmark
[3]Department of Energy and Environmental Biotechnology, National Institute of Genetic Engineering and Biotechnology (NIGEB), Tehran, Iran
Correspondence to: Nosrati H (h.nosrati@modares.ac.ir)

Abstract

Introduction: Dicalcium phosphate dihydrate (DCPD) is a member of the family of calcium phosphates (CP), which has many uses in bone cement. Recently, graphene and its derivatives have been studied to increase the biological and mechanical properties of CP structures and their results have been satisfactory.

Objective: In this study, the main objective is to investigate the physical properties of GO/DCPD powders, which has been synthesized via a simple precipitation method.

Material and Methods: Calcium nitrate tetrahydrate and diammonium hydrogen phosphate were used as a precursor for DCPD synthesis. DCPD was precipitated in the presence of graphene oxide. The powders obtained after washing and drying were evaluated. The analysis performed in the sample includes inductively coupled plasma (ICP), Raman Spectroscopy, Fourier transform infrared spectroscopy (FTIR), X-ray diffraction, Energy dispersive X-ray spectroscopy (EDS), X-ray photoelectron spectroscopy, Field Emission Scanning Electron Microscope (FE-SEM), and high-resolution TEM.

Result: Raman Spectroscopy and XRD results showed that dicalcium phosphate dehydrate formed the hybrid powders along with graphene oxide. DCPD crystallite size was estimated at 138 nm. Microscopic images confirmed the preferred directional growth of DCPD particles. FTIR and XPS results confirmed the emerging bands. ICP and EDS results confirmed the presence of trace elements in the synthesized powders.

Conclusion: According to the above, these powders will have a lot of potential for modifying the properties of bone cement.

Keyword: Tissue Engineering; Calcium Phosphate; Graphene Oxide; Bone Cement; Precipitation

Received: 28 December 2018, Accepted: 14 February 2019

DOI: 10.22034/jtm.2019.173565.1013

Tissues & Biomaterials Research Group

1. Introduction

Recent research on bone tissue engineering has been carried out in various branches of this science [1-6]. Bone defects caused by skeletal diseases, traumatic events, congenital anomalies, and malignancies annually bring millions of patients to hospitals for bone remodeling and transplantation [7, 8]. Bone marrow transplantation by replacing damaged bones with the use of its own patient (autograft) or donors (allograft) has been done since two centuries ago, and autograft is a better option because of high biological acceptance [7, 9]. However, issues such as access restrictions, poisoning of donor sites and increased procedural costs have led research to be found on methods and bio-materials [9].

Among the range of proposed synthetic materials, calcium phosphates (CP) have attracted a lot of attention due to their similar bone composition and excellent properties including biocompatibility, bioactivity, osteoconductivity, and non-immunogenicity, non-toxicity [10-12]. The CP family contains HA, TeCP, α-TCP, β-TCP, DCPD, DCPA, and OCP. One of the applications of this material is coating on metal implants that increase corrosion resistance and biological properties [13], because biological compatibility and biological function of the surface are considered an important issue for biomaterials [14]. Another use of these materials is bone cement [13].

Since the initial formulation in the 1980s, CP cements have been increasingly used as bone substitutes, and many have been commercialized with various compounds. CP cements are produced by a chemical reaction between two phases (solid and liquid) which, when mixed, become doughy and gradually solidifies. The solid phase contains one or more CP compounds. CP is injectable and hardening is achieved in situ through the needle shaped or plate crystal entanglement [7, 8, 15].

These properties make CP cement widely used as fillers in dentistry and orthopedics. It is easily formed and can be easily injected into the cavities with a syringe without the need for an open portal through the tissue [16].

Formulation of composite materials of CPs and resins is difficult as the ceramic usually act as stress concentration centers in resin base composites and cause crack growth [17]. Due to the poor effect of CP particles on the resin matrix, it is important to keep its contents as low as possible without sacrificing the potential for regeneration [18].

Currently, despite the numerous combinations of cement of CP cements, there are only two final products, brushite and apatite, such as HA or CDHA (Calcium Deficient HA), and these two products are further obtained by two types of hydrolysis and acid-reactive chemical reactions. The major difference between these two products is that bromide solubility is 1-2 times higher than apatite solution in physiological pH. However, the bruchite is a metastable phase and may become apatite under physiological conditions [7]. With special conversion processes, Brushite can be converted to monetite with superior Osteoconductive and Osteoinductive properties in vivo. Unfortunately, this cement has shown a decrease in weight, porosity and weakening of mechanical properties in vitro [19].

Brushite, Dicalciumphosphate dehydrates, can be made as hydrolyzed cement with a wide range of applications. In addition to the ability to regenerate bone, it can be replaced in vivo faster than most CPs with reconstructed tissue [20]. It has been used as bioactive filler, with a relatively high solubility with a calcium-phosphorus ratio of 1 and the presence of structural water molecules. One of its interesting features as a filler in repairing composites is that the refractive index is 1.54-1.55, which is better than hydroxyapatite (1.63-1.67) and suitable for photopolymerization [20]. DCPD is low cost and can easily be placed on metal surfaces [21]. CPs must have the same mechanical properties as bone tissue to be used as a substitute for repair agents [22]. One of the ways to improve mechanical properties is to use reinforcements.

Studies on the use of carbon nanomaterials in orthopedic medical applications, especially graphene, have steadily increased during the past 5 years [23-25]. Graphene has excellent mechanical properties (for example, the Young or E modulus) due to the sp^2 carbon bonding network. The single-layer graphene theoretically shows the Young's modulus (E) 1.02 TPa ($\nu = 0.149$) which is approved for a defect-free

Table 1. The primary chemicals used in the powder synthesis phase.

No.	Chem.	Co.	Purity	Formulation
1	Graphene oxide	Abalonyx	25%	G_xO_y
2	Calcium nitrate tetrahydrate	Merck	> 99%	$Ca(NO_3)_2.4H_2O$
3	Diammonium hydrogenphosphate	Merck	> 99%	$(NH_4)_2HPO_4$

graphene sheet with a failure strength of 42 $N.m^{-1}$ [26]. Graphene oxide (GO) is a combination of carbon, oxygen, and hydrogen in variable proportions with a single atomic layer, which is produced by graphite exfoliation with strong oxidants. The bulk product is a solid brown / yellow substance that maintains the structure of the graphite layer, but has a larger, more irregular spacing. The basal plate is decorated with oxygen-containing groups such as hydroxyl, carboxyl and epoxy. GO is hydrophilic and it can be suspended in deionized water, N-Methylpyrrolidinone (NMP), Dimethylformamide (DMF), Tetrahydrofuran (THF) and other solvents that have the same behavior with water as these groups have a higher relative tendency to molecules of water. Graphene oxide can recover most of the properties of pure graphene through its light, heat, or chemical reduction [27- 30].

The chemical depositions of CPs at the graphene nanosheets (GNS) are generally accomplished by dispersing GNS in a chemical bath that CPs are deposited. GNS coated with CPs ensures that CPs and GNS are distributed uniformly. GNS is suspended in calcium carbonate / hydroxide / calcium nitrate in a bath and then mixed together. Then, hydrogen phosphate diammonium / phosphoric acid are added to a highly stirred bath to form a drop in order to create a CP precipitation on a suspended GNS surface. Deposition parameters, such as temperature and pH, should be optimized to ensure that the desirable phase is formed HA, $CaHPO_42H_2O$ or $Ca_3(PO_4)_2$ phases. GNS is uniformly distributed in CPs precipitation to powder form via chemical deposition [31- 35].

Williamson-Hall method was used to calculate the crystallite size (Equation 1):

$$\beta.\text{Cos}\,\theta=\frac{(0.9\lambda)}{d}+2\eta.\text{Sin}\,\theta \qquad (1)$$

Where d is grain size, θ is Bragg diffraction angle, λ is wave length of used X-ray (Cu), β is full width at half height (FWHM), and η is crystalline lattice strain.

Recently, graphene and its derivatives have been studied to increase the biological and mechanical properties of CP structures and their results have been satisfactory [36- 39]. In this study, the main objective is to investigate the physical properties of GO/DCPD powders, which has been synthesized via a simple precipitation method and has not been addressed so far. According to the above, these powders will have a lot of potential for modifying the properties of bone cement.

2. Materials and Methods

The primary chemicals used in the powder synthesis phase with the specifications are listed in Table 1.

2.1. Powders synthesis

For synthesis of powders, solutions containing calcium and phosphorus were prepared with calcium to phosphorus ratio of >1. For this purpose, 2.5 g of $(Ca(NO_3)_2.4H_2O)$ in 110 cm^3 distilled water and 1 g of $((NH_4)_2HPO_4)$ in 75 cm^3 distilled water were prepared as solutions. First, the solution containing calcium was added dropwise to 20 mL of GO colloid (5 mg/mL) and was stirred for an hour. Then, the solution containing phosphorus was added dropwise to the above solution. The process was assessed by analyzing the precipitated powders after drying.

2.2. Characterization

Phase constituents of the samples were identified by X-ray diffraction (XRD, X' Pert Pro, Panalytical Co.) with a detector using Cu Kα radiation (λ=1.5406 Å) generated at 40 kV and 40 mA and a 2θ scanning range from 5° up to 80° in steps of 0.02°. The

Fourier transform infrared spectroscopy (FTIR, VERTEX 70, Brucker Co.) was carried out to identify the functional groups of the composites with a resolution of 4 cm^{-1} and a scan number of 8, with a spectral region from 400 to 4000 cm^{-1} using 2 cm^{-1} steps. The samples were prepared and mixed with potassium bromide (KBr) in a concentration of 1 mg powdered samples and 300 mg KBr. The mixture was pressed into discs having 1 mm thickness by applying 200 MPa pressures. The spectra were collected at room temperature (25 °C) and 60% relative humidity. Micro-Raman spectra were carried out using a Reinshaw invia spectrometer in the range of 250-1200 cm^{-1} (recording 5 times for 10 seconds of each accumulation) with a wavelength of 532 nm (green laser line in a backscattering configuration using a microscope with a 100× objective, 100% power) and an acquisition time of 10 s, which had been excited from an argon ion laser. An optical microscope was used with the Raman spectrometer. In order to remove the fluorescence background, which is a serious challenge in the Raman analysis of apatite, the samples were subjected on Al foil.

The morphology of the powders was observed by a Field Emission Scanning Electron Microscope (FESEM, Hitachi S4700 equipped with energy dispersive X-ray spectroscopy) and a Portable Scanning Electron Microscope (SEM, TM-1000). The samples were mounted in an adhesive carbon film and Au coated by sputtering for its observation.

HRTEM images were obtained on a TALOS F200A with a twin lens system, X-FEG electron source, Ceta 16M camera and a super-X EDS detector. Spatially resolved elemental analysis, with a spatial resolution higher than 2 nm, was obtained using the same TALOS microscope in STEM mode.

The other instruments used to characterize the samples include: inductively coupled plasma (ICP) (DV7300, Optima Co.), TEM (CM120, Philips), FTIR (VERTEX 70, Brucker Co.), and X-ray photoelectron spectroscopy (XPS).

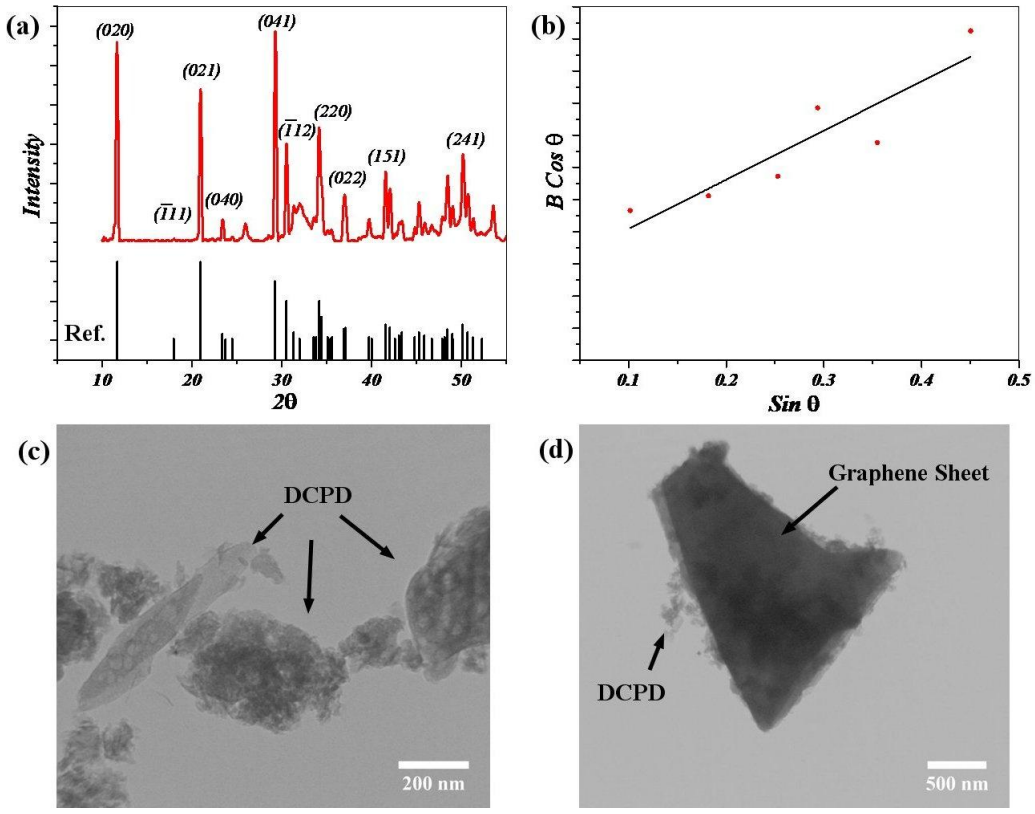

Figure 1. The XRD and TEM images of the hybrid powders after precipitation process.

3. Results and Discussion

The XRD pattern and TEM images of the hybrid powders after precipitation process is shown in Figure 1. The structure of powders, with its x-ray pattern shown in Figure1a, is monoclinic (JCPDS 72-0713). The crystallite size according to this pattern, Williamson Hal method is about 138 nm (Figure 1b). The characteristic peak of GO (2θ=10) is covered with the peak of the (020) diffraction surface [41, 42]. In addition, there are no signs of graphite peaks due to the presence of DCPD peaks in their vicinity and their small content GO, while their presence is confirmed by TEM, which indicates that GO composition has no effect on stability of the DCPD and the absence of GO peaks is likely to be related to the reduced graphene oxide layer structure partially. TEM images show the GO which is composed of DCPD deposit on its surfaces. These images also confirm the directional growth of DCPD that the particle size is between 100 and 200 nm.

Figure 2 shows the HRTEM, FFT and IFFT analysis of hybrid powders after precipitation process. HRTEM analysis images confirm the presence of GO layers in final powders. The distance between the carbon atoms is 0.14 nm. Changing the mode in two FFT images is due to the GO surface folding and wrinkling.

Figure 3 shows the schematic diagram for DCPD/GO interaction in hybrid powders. According to XRD-analysis, the d-spacing of (020) planes in DCPD are 0.76 nm. The distance between the GO sheets is 0.83 nm in cross section. So, mismatch for this state is much less than the incoherent limitation (0.25). Therefore, the interface between the two phases is coherent.

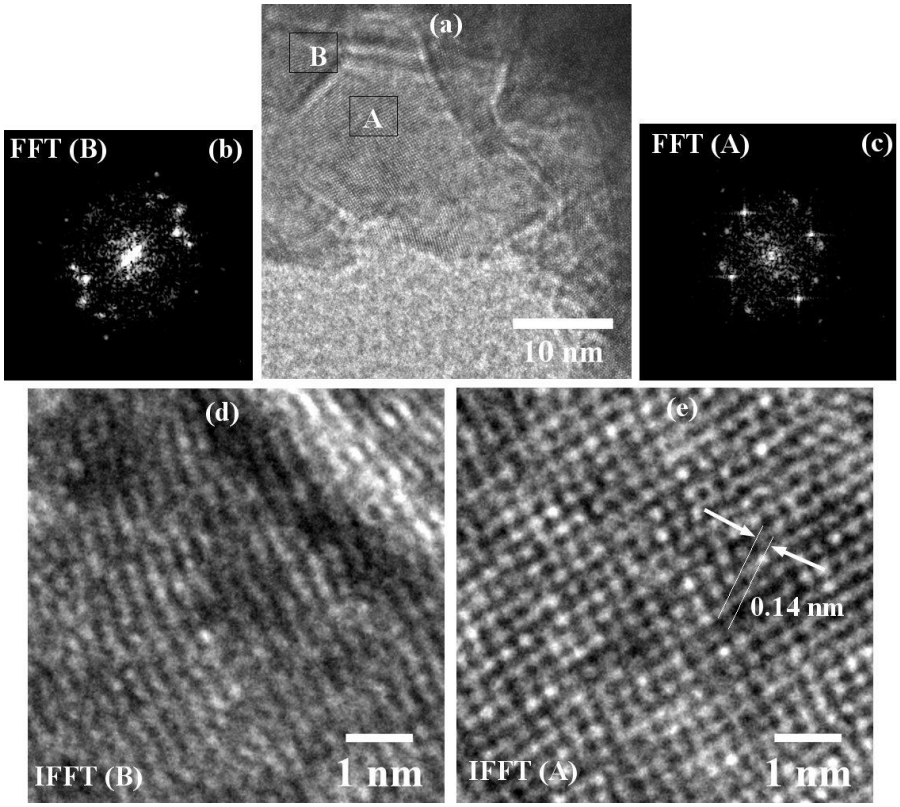

Figure 2. HRTEM, FFT, and IFFT analysis of GO sheets.

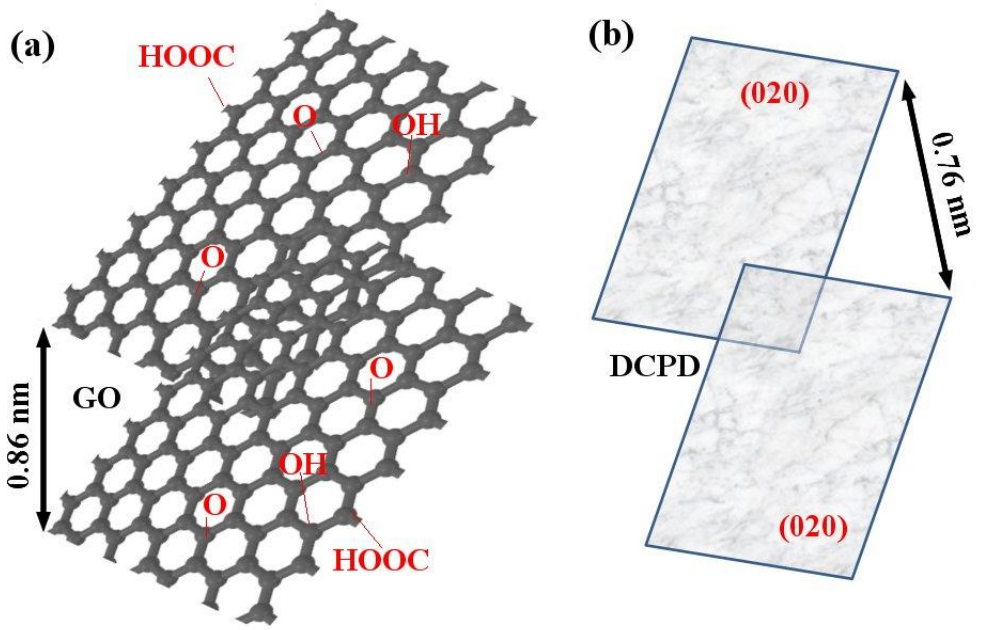

Figure 3. Schematic diagram for DCPD/GO interaction in hybrid powders.

Figure 4 shows the FTIR spectrum of GO, starting materials, and final samples along with XPS spectra of the GO/DCPD powders. In FTIR analysis, two conditions have been investigated, the first one is when GO is doped with Ca ions and then the phosphorus ions are added to it. In the second one, phosphorous ions are first added to GO. In both cases, the DCPD eventually precipitates (Figure 4a). But, when calcium ions are first mixed with GO, there will probably be more bonds between Ca ions and GO because calcium ions have a negative charge and are more absorbed by GO. However, phosphorous ions are also partially absorbed by GO [47]. Figure 4b shows the FTIR spectrum of powders after precipitation. The wide absorption peak between 2500 cm^{-1} and 3500 cm^{-1} is related to the stretching vibrations of the O-H band. Absorption peak in 1650 cm^{-1} is due to bending of H-O-H and the one at 1065 cm^{-1},1130 cm^{-1} and 1215 cm^{-1} are related to stretching vibrations of the O=P band. Absorption peaks at 980 cm^{-1},870 cm^{-1} and 790 cm^{-1} are related to the P-O-P asymmetric stretching vibrations while the peaks in 525cm^{-1} and 580 $cm^{-1}$are due to (H-O-) P=O for acid phosphates [43, 48, 49]. Due to the presence of GO in the initial solution, the peaks associated with this material and the peaks associated with the DCPD are likely to be overlapping.

Figures 4c, d show the XPS spectra of the GO/DCPD powders. The GO spectrum should contain carbon (284- 289 eV) and oxygen. The emergence of other couriers including Ca 2p (350) are signs of DCPD formation (Figure 4c) [45]. The high resolution XPS spectrum of O 1s of the GO- DCPD powders is shown in Figure 4d, in which the peak centered at 531 eV is attributed to the O in DCPD and OH groups, whereas those at 533 and 532 eV correspond to the O in C–O and H-C=O groups [46]. The XPS results further reveal the presence of DCPD and GO, which agree with the Raman analysis results.

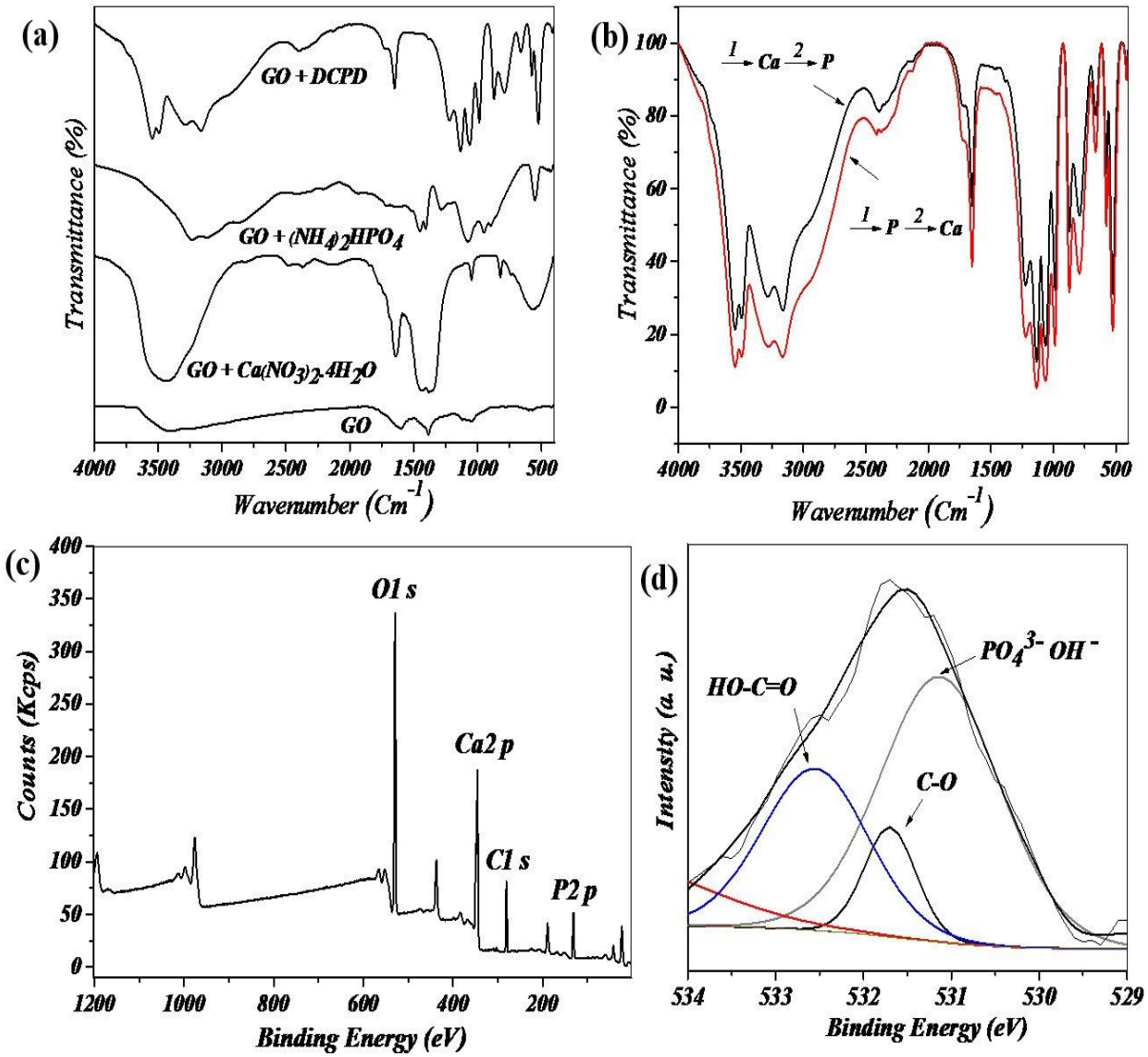

Figure 4. (a, b) The FTIR spectrum of GO, starting materials, and final samples, (c, d) XPS spectra of the GO/DCPD powders.

Figure 5 shows FESEM images for the final hybrid powders. Figure 5a shows plate-shaped DCPD particles, which have grown preferentially and in certain directions. Figures 5b and 5c show DCPD particles at higher magnifications, which are evidence of their directional growth. Figure 5d shows FESEM image of GO layers which are composed of a DCPD deposit on its surface. In a study published by other researchers, the directional growth of DCPD is mentioned [40].

Figure 6 shows the Raman spectrum of the hybrid powders after precipitation process. The main bonds in Figure 6b spectrum are the phosphate bonds. DCPD Raman vibrations are associated with four different modes of four internal tetragonal states. ν_1 correspond to a totally symmetric stretching mode of the tetrahedral PO_4^{3-} group (P-O bond). ν_2 is a doubly degenerate bending mode of the phosphate group (P-O-P bond). ν_3 is a triply degenerate asymmetric stretching mode of the tetrahedral PO_4^{3-} group (P-O bond), and ν_4 is a triply degenerate bending mode of the PO_4 group (O-P-O) [43, 46]. All three shifts obtained in G, 2D and D (Figure 6a, c) are related to carbon compounds such as GO. In fact, these shifts along with previous microscopic images are the best evidence of the presence of GO compounds in the final synthesized powders.

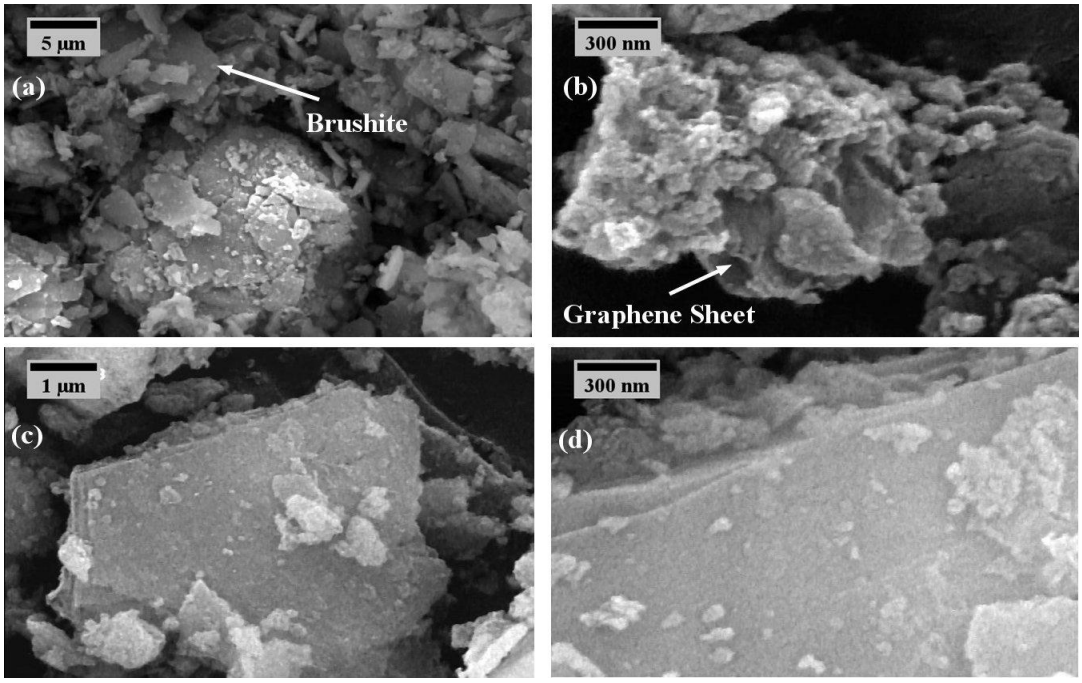

Figure 5. FESEM images of the final hybrid powders.

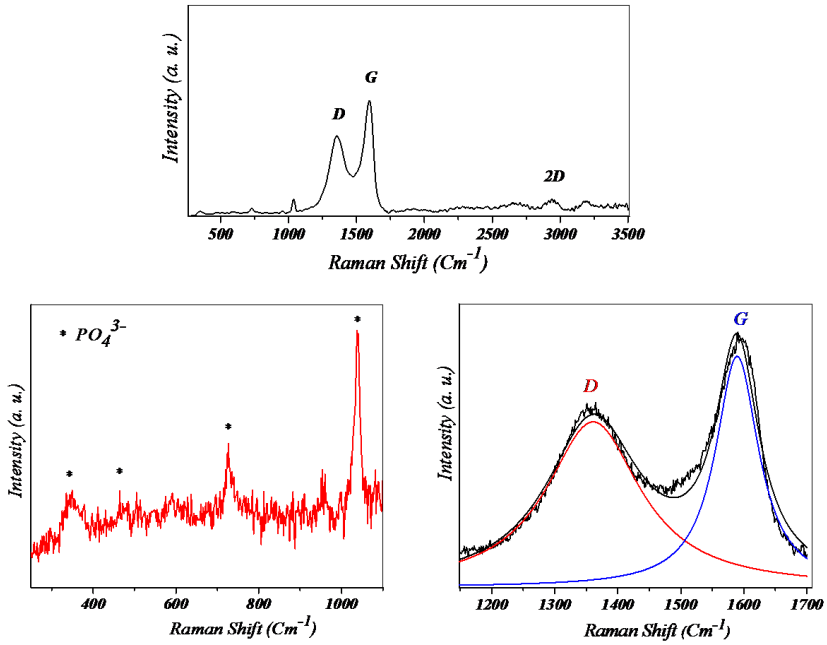

Figure 6. Raman spectrum of the hybrid powders after precipitation process

Figure 7 shows the energy dispersive X-ray spectroscopy analysis, and map images for the final hybrid powders. The EDS analysis confirms the presence of trace elements in the synthesized

composite which is accordance with the ICP analysis. The following reaction occurs in this mechanism, in which the final solution, S, contains some residual calcium and phosphorus ions:

$$Ca(NO_3)_2.4H_2O+(NH_4)_2HPO_4+H_2O \rightarrow CaHPO_4.2H_2O+S \quad (1)$$

The first analysis was inductively coupled plasma mass spectrometry (ICP-MS) of the final solution(S) which indicated that almost the ratio of calcium to phosphate should be 1.

In the sample, the powders were easily separated by centrifugation. Based on the findings of the characterization, a large number of primary ions have not reacted at this stage and the ratio of calcium to phosphorous in these powders was approximately 1. Also, the map of the elements shows that the trace elements are dispersed homogeneously in the powders.

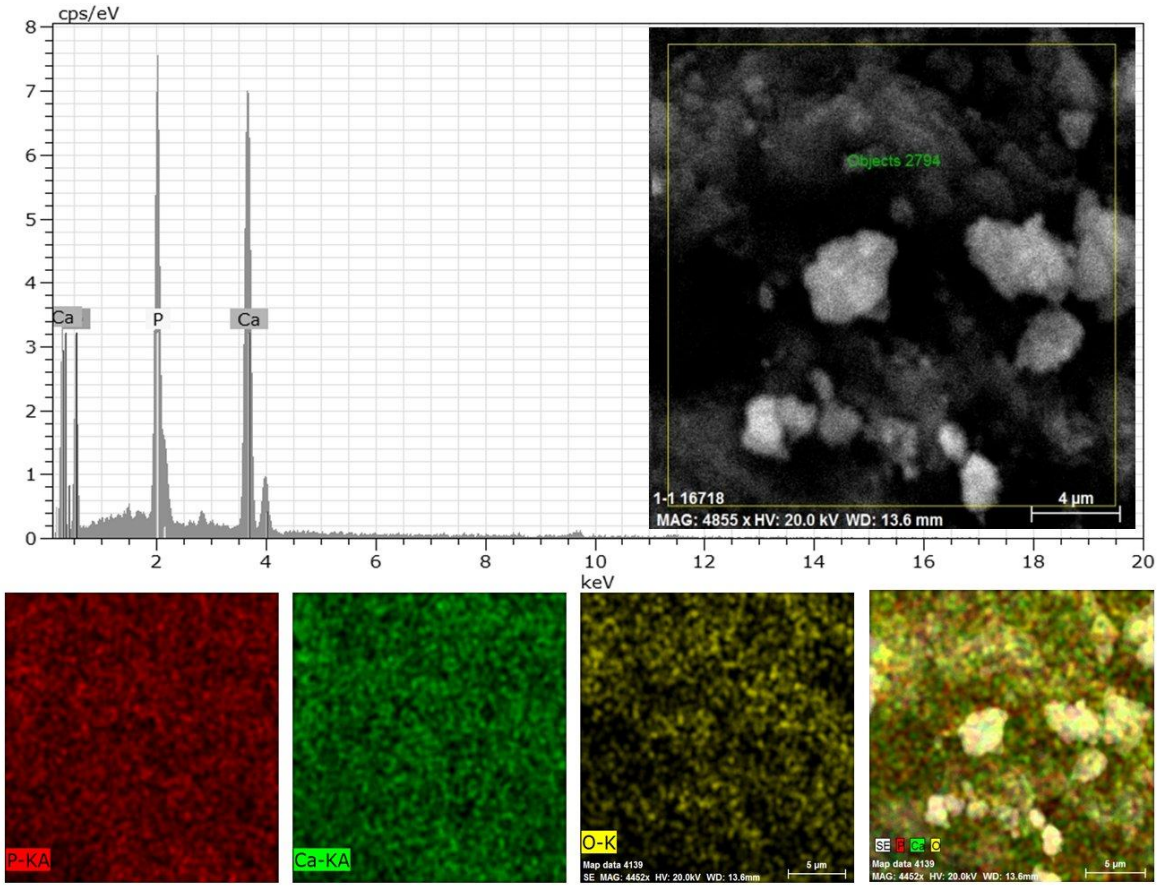

Figure 7. Energy dispersive X-ray spectroscopy analysis, and map images for the final hybrid powders.

Figure 8 shows the mechanism of nanostructured powders formation by precipitation. GO basal planes are more covered with epoxy and hydroxyl groups, while carboxyl groups (-COOH or COO) are located at the edges. The charge of the GO surface is negative in terms of functional groups. The structure of GO affects the formation of DCPD and induces epitaxial and directional growth. Also, as anchoring sites, oxygen-containing groups induce the formation and bonding of particles to the surface of GO. In the chemical precipitation, when adding calcium nitrate to a solution containing GO, Ca^{2+} cations are absorbed and bound to GO by electrostatic interactions with hydroxyl groups (C-O-C, OH) or ion exchange with carboxyl groups (H^{+}) and play the role of the primary sites for nucleation and growth of DCPD particles. Calcium ions can react in situ with phosphate ions and form calcium phosphate nanoparticles through electrovalence reactions. In this process, the solution is strongly stirred and the GO layers are homogeneously dispersed, then the same nucleation and the controlled growth occur.

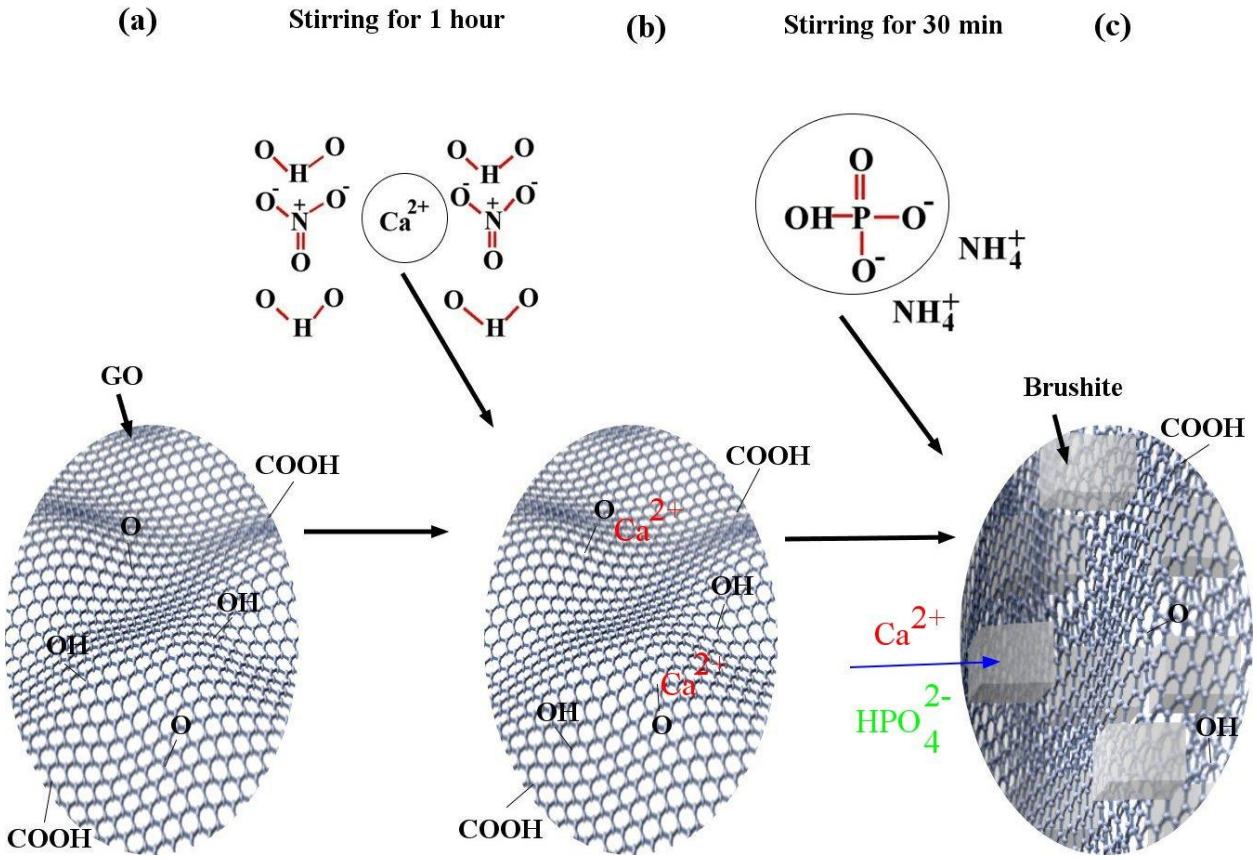

Figure 8. mechanism of nanostructured powders formation by precipitation method. a) GO. b) GO+Ca^{2+}. c) GO+DCPD

4. Conclusion

Dicalcium phosphate dihydrate was precipitated in the presence of graphene oxide. Raman Spectroscopy and XRD results showed that dicalcium phosphate dehydrate (DCPD) formed the hybrid powders along with graphene oxide. DCPD crystallite size was estimated at 138 nm. Microscopic images confirmed the preferred directional growth of DCPD particles in plate-shaped. FTIR and XPS results confirmed the emerging bands. ICP and EDS results confirmed the presence of trace elements in the synthesized powders. The result of this study is likely to improve the biological and mechanical properties of bone cements.

Conflict of interest

The authors declare that they have no conflict of interests.

Acknowledgments

None declared.

References

[1] FS. Hosseini, F. Soleimanifar, A. Aidun, SE. Enderami, E. Saburi, H. Z. Marzouni, M-M. Khani, A. Khojasteh, A. Ardeshirylajimi, Poly (3-hydroxybutyrate-co-3-hydroxyvalerate) improved osteogenic differentiation of the human induced pluripotent stem cells while considered as an artificial extracellular matrix, Journal of Cellular Physiology, 2018, https://doi.org/10.1002/jcp.27807.

[2] M. Jafarkhani, Z. Salehi, A. Aidun, MA. Shokrgozar, Bioprinting in Vascularization Strategies, ibj, 23, 1, 2019, pp 9- 20.

[3] [3] F. Ghorbani, A. Zamanian, A. Aidun, Bioinspired polydopamine coating-assisted electrospun polyurethane-graphene oxide nanofibers for bone tissue engineering application, Journal of Applied Polymer Science, 2019, https://doi.org/10.1002/app.47656

[4] A. Aidun, A. Zamanian, F. Ghorbani, Novel bioactive porous starch–siloxane matrix for bone regeneration: Physicochemical, mechanical, and in vitro properties, Biotechnology and applied biochemistry, 66, 2019, DOI: 10.1002/bab.1694

[5] H. Nosrati, R. Sarraf Mamoory, F. Dabir, M. Canillas Perez, M. A. Rodriguez, D. Q. Svend Le, C. E. Bunger, In situ synthesis of three dimensional graphene-hydroxyapatite nano powders via hydrothermal process, Materials Chemistry and Physics, 2019, 222, pp 251–255, https://doi.org/10.1016/j.matchemphys.2018.10.023

[6] H. Nosrati, R. Sarraf Mamoory, F. Dabir, D. Q. Svend Le, C. E. Bunger, M. Canillas Perez, M. A. Rodriguez, Effects of hydrothermal pressure on in situ synthesis of 3D graphene/hydroxyapatite nano structured powders, Ceramics International, 2019, 45, pp 1761–1769, https://doi.org/10.1016/j.ceramint.2018.10.059

[7] Jingtao Zhang, Weizhen Liu, Verena Schnitzler, Franck Tancret, Jean-Michel Bouler, Calcium phosphate cements for bone substitution: Chemistry, handling and mechanical properties, Acta Biomaterialia, 10 (2014) 1035–1049, https://doi.org/10.1016/j.actbio.2013.11.001

[8] Yang Xia, Huimin Chen, Feimin Zhang, Chongyun Bao, Michael D. Weir, Mark A. Reynolds, Junqing Ma, Ning Gu, Hockin H.K. Xu, Gold nanoparticles in injectable calcium phosphate cement enhance osteogenic differentiation of human dental pulp stem cells, Nanomedicine: Nanotechnology, Biology, and Medicine 14 (2018) 35–45, https://doi.org/10.1016/j.nano.2017.08.014

[9] Zeeshan Sheikh, Yu Ling Zhang, Faleh Tamimi, Jake Barralet, Effect of processing conditions of dicalcium phosphate cements on graft resorption and bone formation, Acta Biomaterialia 53 (2017) 526–535, https://doi.org/10.1016/j.actbio.2017.02.022

[10] Maria Giovanna Gandolfi, Fausto Zamparini, Micaela Degli Esposti, Federica Chiellini, Conrado Aparicio, Fabio Fava, Paola Fabbri, Paola Taddei, Carlo Prati, Polylactic acid-based porous scaffolds doped with calcium silicate and dicalcium phosphate dihydrate designed for biomedical application, Materials Science & Engineering C 82 (2018) 163–181, https://doi.org/10.1016/j.msec.2017.08.040

[11] Khairul Anuar Shariff , Kanji Tsuru , Kunio Ishikawa, Fabrication of dicalcium phosphate dihydrate-coated β-TCP granules and evaluation of their osteoconductivity using experimental rats, Materials Science and Engineering C 75 (2017) 1411–1419, https://doi.org/10.1016/j.msec.2017.03.004

[12] Alexandra Ioana Bucur, Raul Alin Bucur, Zoltan Szabadai, Cristina Mosoarca, Petrica Andrei Linul, Influence of small concentration addition of tartaric acid on the 220 °C hydrothermal synthesis of hydroxyapatite, Materials Characterization 132 (2017) 76-82,

https://doi.org/10.1016/j.matchar.2017.07.047

[13] Agnese Carino, Christian Ludwig, Antonio Cervellino, Elisabeth Müller, Andrea Testino, Formation and transformation of calcium phosphate phases under biologically relevant conditions: Experiments and modeling, Acta Biomaterialia 74 (2018) 478–488, https://doi.org/10.1016/j.actbio.2018.05.027

[14] Xia Li, Zhengyang Weng, Wei Yuan, Xianzi Luo, Hoi Man Wong, Xiangmei Liu,Shuilin Wu, K.W.K. Yeung, Yufeng Zheng, Paul. K. Chu, Corrosion resistance of dicalcium phosphatedihydrate/poly (lactic-co-glycolic acid) hybrid coating on AZ31magnesium alloy, Corrosion Science 102 (2016) 209–221, https://doi.org/10.1016/j.corsci.2015.10.010

[15] Hockin HK Xu1, Ping Wang, Lin Wang, Chongyun Bao, Qianming Chen, Michael D Weir, Laurence C Chow, Liang Zhao, Xuedong Zhou5 and Mark A Reynolds, Calcium phosphate cements for bone engineering and their biological properties, Bone Research (2017) 5, 17056, 1-19, https://doi.org/10.1038/boneres.2017.56

[16] Chia-Ling Ko, Jian-Chih Chen, Chun-Cheng Hung, Jen-ChyanWang, Yin-Chun Tien,Wen-Cheng Chen , Biphasic products of dicalcium phosphate-rich cement with injectability and nondispersibility, Materials Science and Engineering C 39 (2014) 40–46, https://doi.org/10.1016/j.msec.2014.02.033

[17] Livia C. Natale, Marcela C. Rodrigues, Yvette Alania, Marina D.S. Chiari, Leticia C.C. Boaro, Marycel Cotrim, Oscar Vega, Roberto R. Braga, Mechanical characterization and ion release of bioactive dental composites containing calcium phosphate particles, Journal of the Mechanical Behavior of Biomedical Materials 84 (2018) 161–167, https://doi.org/10.1016/j.jmbbm.2018.05.022

[18] Marina D.S. Chiari, Marcela C. Rodrigues, Tathy A. Xavier, Eugen M.N. de Souza, Victor E. Arana-Chavez, Roberto R. Braga, Mechanical properties and ion release from bioactive restorative composites containing glass fillers and calcium phosphate nano-structured particles, dental materials 31 (2015) 726–733, https://doi.org/10.1016/j.dental.2015.03.015

[19] Zeeshan Sheikh, Yu Ling Zhang, Liam Grover, Géraldine E. Merle, Faleh Tamimi, Jake Barralet, In vitro degradation and in vivo resorption of dicalcium phosphate cement based grafts, Acta Biomaterialia 26 (2015) 338–346, https://doi.org/10.1016/j.actbio.2015.08.031

[20] Faleh Tamimi, Damien Le Nihouannen, Hazem Eimar, Zeeshan Sheikh, Svetlana Komarova, Jake Barralet, The effect of autoclaving on the physical and biological properties of dicalcium phosphate dihydrate bioceramics: Brushite vs. monetite, Acta Biomaterialia 8 (2012) 3161–3169, https://doi.org/10.1016/j.actbio.2012.04.025

[21] Daniel Kajánek, Filip Pastorek, Stanislava Fintová, Adrián Bača, Study of corrosion behavior of dicalcium phosphate-dihydrate (DCPD) coating prepared by large amplitude sinusoidal voltammetry (LASV) technique on ZW3 magnesium alloy, Procedia Engineering 192 (2017) 399 – 403, https://doi.org/10.1016/j.proeng.2017.06.069

[22] Ingrid Ajaxon, Alice Acciaioli, Giacomo Lionello, Maria-Pau Ginebra, Caroline Öhman-Mägi, Massimiliano Baleani, Cecilia Persson, Elastic properties and strain-to-crack-initiation of calcium phosphate bone cements: Revelations of a high-resolution measurement technique, Journal of the Mechanical Behavior of Biomedical Materials 74 (2017) 428–437, https://doi.org/10.1016/j.jmbbm.2017.06.023

[23] Janković, A., Eraković, S., Mitrić, M., Matić, I. Z., Juranić, Z. D., Tsui, G. C., Tang, C.-y., Mišković-Stanković, V., Rhee, K. Y., & Park, S. J., Bioactive Hydroxyapatite/Graphene Composite Coating and Its Corrosion Stability in Simulated Body Fluid, Journal of Alloys and Compounds, 624 (2015) 148-157, https://doi.org/10.1016/j.jallcom.2014.11.078

[24] Lahiri, D., Ghosh, S., & Agarwal, A., Carbon nanotube reinforced hydroxyapatite composite for orthopedic application: A review, Materials Science and Engineering: C, 32(7), (2012), 1727-1758, https://doi.org/10.1016/j.msec.2012.05.010

[25] Zhang, L., Liu, W., Yue, C., Zhang, T., Li, P., Xing, Z., & Chen, Y., A tough graphene nanosheet/hydroxyapatite composite with improved in vitro biocompatibility, Carbon, 61, (2013), 105-115, https://doi.org/10.1016/j.carbon.2013.04.074

[26] Lee, C., Wei, X., Kysar, J. W., & Hone, J., Measurement of the elastic properties and intrinsic strength of monolayer graphene, science, 321(5887), (2008), 385-388, http://doi.org/10.1126/science.1157996

[27] Dreyer, D. R., Park, S., Bielawski, C. W., & Ruoff, R. S., The chemistry of graphene oxide, Chemical Society Reviews, 39(1), (2010), 228-240, https://doi.org/10.1039/B917103G

[28] Hu, W., Peng, C., Luo, W., Lv, M., Li, X., Li, D., Huang, Q., & Fan, C., Graphene-based antibacterial

paper, ACS nano, 4(7), (2010), 4317-4323, https://doi.org/10.1021/nn101097v

[29] Kim, J., Cote, L. J., Kim, F., Yuan, W., Shull, K. R., & Huang, J., Graphene oxide sheets at interfaces. Journal of the American Chemical Society, 132(23), (2010), 8180-8186, https://doi.org/10.1021/ja102777p

[30] Zhu, Y., Murali, S., Cai, W., Li, X., Suk, J. W., Potts, J. R., & Ruoff, R. S., Graphene and graphene oxide: synthesis, properties, and applications, Advanced Materials, 22(35), (2010), 3906-3924, https://doi.org/10.1002/adma.201001068

[31] Li, M., Wang, Y., Liu, Q., Li, Q., Cheng, Y., Zheng, Y., Xi, T., & Wei, S., In situ synthesis and biocompatibility of nano hydroxyapatite on pristine and chitosan functionalized graphene oxide. Journal of Materials Chemistry B, 1(4), (2013), 475-484, https://doi.org/10.1039/C2TB00053A

[32] Liu, Y., Dang, Z., Wang, Y., Huang, J., & Li, H., Hydroxyapatite/graphene-nanosheet composite coatings deposited by vacuum cold spraying for biomedical applications: Inherited nanostructures and enhanced properties, Carbon, 67, (2014), 250-259, https://doi.org/10.1016/j.carbon.2013.09.088

[33] Neelgund, G. M., Oki, A., & Luo, Z., In situ deposition of hydroxyapatite on graphene nanosheets, Materials Research Bulletin, 48(2), (2013), 175-179, https://doi.org/10.1016/j.materresbull.2012.08.077

[34] Núñez, J. D., Benito, A. M., González, R., Aragón, J., Arenal, R., & Maser, W. K., Integration and bioactivity of hydroxyapatite grown on carbon nanotubes and graphene oxide, Carbon, 79, (2014), 590-604, https://doi.org/10.1016/j.carbon.2014.08.020

[35] Oyefusi, A., Olanipekun, O., Neelgund, G. M., Peterson, D., Stone, J. M., Williams, E., Carson, L., Regisford, G., & Oki, A., Hydroxyapatite grafted carbon nanotubes and graphene nanosheets: Promising bone implant materials, Spectrochimica Acta Part A: Molecular and Biomolecular Spectroscopy, 132, (2014), 410-416, https://doi.org/10.1016/j.saa.2014.04.004

[36] Fan, Z., Wang, J., Wang, Z., Ran, H., Li, Y., Niu, L., Gong, P., Liu, B., & Yang, S., One-pot synthesis of graphene/hydroxyapatite nanorod composite for tissue engineering, Carbon, 66, (2014), 407-416, https://doi.org/10.1016/j.carbon.2013.09.016

[37] Qi, C., Zhu, Y.-J., Ding, G.-J., Wu, J., & Chen, F., Solvothermal synthesis of hydroxyapatite nanostructures with various morphologies using adenosine 5′-monophosphate sodium salt as an organic phosphorus source, RSC Advances, 5(5), (2015), 3792-3798, https://doi.org/10.1039/C4RA13151G

[38] Jeong-Woo Kim, Yong Cheol Shin, Jin-Ju Lee, Eun-Bin Bae, Young-Chan Jeon, Chang-Mo Jeong, Mi-Jung Yun, So-Hyoun Lee, Dong-Wook Han, and Jung-Bo Huh, The Effect of Reduced Graphene Oxide-Coated Biphasic Calcium Phosphate Bone Graft Material on Osteogenesis, Int. J. Mol. Sci. (2017), 18, 1725; https://doi.org/10.3390/ijms18081725

[39] Jun Jae Lee, Yong Cheol Shin, Su-Jin Song, Jae Min Cha, Suck Won Hong, Young-Jun Lim, Seung Jo Jeong, Dong-Wook Han, and Bongju Kim, Dicalcium Phosphate Coated with Graphene Synergistically Increases Osteogenic Differentiation In Vitro, Coatings (2018), 8, 13; https://doi.org/10.3390/coatings8010013

[40] T.K. Anee, N. Meenakshi Sundaram, D. Arivuoli, P. Ramasamy, S. Narayana Kalkura, Influence of an organic and an inorganic additive on the crystallization of dicalcium phosphate dihydrate, Journal of Crystal Growth 285 (2005) 380–387, https://doi.org/10.1016/j.jcrysgro.2005.08.036

[41] M. Landin, R.C. Rowe, P. York, Structural changes during the dehydration of dicalcium phosphate dihydrate, European Journal of Pharmaceutical Sciences 2 (1994) 245-252, https://doi.org/10.1016/0928-0987(94)90029-9

[42] Wen-Cheng Chen, Kai-Chi Chang, Hui-Yu Wu, Chia-Ling Ko, Chien-Lin Huang, Thermal cycling effect of dicalcium phosphate-reinforced composites on auto-mineralized dental resin, Materials Science and Engineering C 45 (2014) 359–368, https://doi.org/10.1016/j.msec.2014.09.032

[43] Jingwei Xu, Ian S. Butler, Denis F.R. Gilson, FT-Raman and high-pressure infrared spectroscopic studies of dicalcium phosphate dihydrate (CaHPO4•2H2O) and anhydrous dicalcium phosphate (CaHPO4), Spectrochimica Acta Part A 55 (1999) 2801–2809, https://doi.org/10.1016/S1386-1425(99)00090-6

[44] M. Santana, J. O. Estevez, and V. Agarwal, Room Temperature Crystallization of Hydroxyapatite in Porous Silicon Structures, Nanoscale Res Lett, 11: 497, (2016), https://doi.org/10.1186/s11671-016-1658-4

[45] Yingchao Su, YuntingGuo, Zilong Huang, Zhihui Zhang, Guangyu Li, JiansheLian, Luquan Ren, Preparation and corrosion behaviors of calcium

phosphate conversion coating on magnesium alloy, Surface & Coatings Technology 307 (2016) 99–108, https://doi.org/10.1016/j.surfcoat.2016.08.065

(1998) 15–27, https://doi.org/10.1016/S0927-7765(98)00014-9

[47] Xiaochang Qiao, Shijun Liao, Chenghang You and Rong Chen, Phosphorus and Nitrogen Dual Doped and Simultaneously Reduced Graphene Oxide with High Surface Area as Efficient Metal-Free Electrocatalyst for Oxygen Reduction, Catalysts (2015), 5, 981-991; https://doi.org/10.3390/catal5020981

[48] Lizhi He, Zude Feng, Preparation and characterization of dicalcium phosphate dihydrate coating on enamel, Materials Letters 61 (2007) 3923–3926, https://doi.org/10.1016/j.matlet.2006.12.059

[49] Bouzid Mohammed, Djadi Amina and Guechtoulli Samira, The Dicalcium Phosphate Dihydrate Fixator and Stabilizer of Glutaraldehyde, Journal of Materials Science and Engineering B 3 (9) (2013) 605-611, https://doi.org/10.1002/9781118995433.ch23

[46] C. Combes, C. Rey, M. Freche, XPS and IR study of dicalcium phosphate dihydrate nucleation ontitanium surfaces, Colloids and Surfaces B: Biointerfaces 11